Process–Structure Control in AA5754-H111/Dual-Phase Steel Friction Stir Spot Welds

Phillip Harris Paul[1,*] and Andrew Martin[1]

[1] Lawrence Livermore National Laboratory, 7000 East Avenue, Livermore, California 94550
* Correspondence: paul_harris@gse.harvard.edu

Abstract: The key problem of the spot joining technology based on the use of aluminum and steel as components is to create an extended mechanically effective bonding area without formation of brittle Fe-Al reaction layers and undesirable geometry of hooks. The present study explores the process of friction stir spot welding of 2 ± 0.2 mm AA5754-H111 aluminum alloy to 3 mm Strenx 960 DP steel under different combinations of two ferrite-martensite steel structures obtained by intercritical heat treatment (IHT) at 725 °C and 775 °C followed by quenching, and three tool rotational velocities. Volume content of martensite after IHT and water quenching reached 0.38 and 0.61, correspondingly, while hardness values equaled 327 and 377 HV. Welds have been performed by means of a 4 mm cylindrical WC-Co pin, 12 mm flat shoulder, plunging rate of 12 mm/min, zero tilt of the tool axis to the surface of material being welded, 3 s dwell time and 0.7 mm penetration into the steel at rotational speeds of 800, 1200, and 2000 rpm. What are the roles of rotational speed and microstructure of initially used steel in governing process load, annular bond formation, hook shape evolution, structural transformations in steel, hardness variations, and brittle intermetallic compounds? An increment in rotational velocity resulted in a considerable decrease of the representative value of peak plunging force from about 16.5 kN at 800 rpm to about 10.4 kN at 2000 rpm proving that heating and plastic softening due to friction were the predominant factors here. Microstructure of initially applied steel did not significantly influence the peak plunging load for the selected range of speeds, but played an important role in formation of final structure. High-martensite IHT775 steel was responsible for the increase of hook heights at 1200 and 2000 rpm, while low-martensite IHT725 steel demonstrated the highest growth in width of bond at 2000 rpm. Martensitic stir zone has been revealed in the steel below exit hole, which afterwards became thermomechanically and thermally affected zones approaching the initial ferrite-martensite ratio. Reaction products of Fe-Al interfacial layers have been detected at tips of hooks, along the interface of the exit hole and at its corner. Hardness of intermetallic compounds varied in range 456 to 937 $HV_{0.1}$, brittle nature was proved by local crack formation. The results show that rotation speed should be high for minimizing forces and forming bonds, although it works under the conditions of controlling hook formation and chemical reactions occurring at the interface.

Keywords: friction stir spot welding; AA5754-H111; dual-phase steel; Strenx 960; aluminum-steel joining; hook morphology; bond width; martensitic transformation; microhardness; Fe–Al intermetallic compounds; process window

Citation: Phillip Harris Paul and Andrew Martin. 2022. Process–Structure Control in AA5754-H111/Dual-Phase Steel Friction Stir Spot Welds. *TK Techforum Journal (ThyssenKrupp Techforum)* 2022(2): 1–17.

Received: April-07-2022
Accepted: July-01-2022
Published: September-30-2022

1. Introduction

Combining aluminum alloys and advanced steels has emerged as a practical strategy for saving structural weight while maintaining stiffness, crashworthiness, and production efficiency. Automotive body structures, transport vehicles, and light-weight load-bearing systems use a mixture of aluminum alloy and high-strength steels for local performance requirements that cannot be satisfied using either material alone. In general, aluminum alloy excels in outer panel applications due to the combination of low density and excellent

formability, while dual-phase steels are used in parts subjected to concentrated deformations or impacts. The engineering benefit provided by such material combinations is not only determined by the material selections themselves but also depends on the local joining technology because a weak, brittle, or unstable joint will render any material substitution irrelevant [1–4].

The current work focuses on aluminum and steel materials because such a combination poses a standard example of the challenge faced in joining technologies. AA5754-H111 is a precipitation-free alloy with excellent corrosion resistance, good formability, and moderate yield strength. Strenx 960, in turn, is a high-strength steel alloy exhibiting significantly higher strengths and a ferrite/martensite transformation-dependent microstructure. Jointing aluminum to steel involves many challenges, namely plasticization of aluminum, local contact and deformation of steel, and limitation of Fe-Al reaction during the process. The particular combination examined here can be considered beneficial for studying the relationship between process parameters and microstructural outcomes, since it involves a relatively soft aluminum alloy covered with oxide layer, and hard ferrite/martensite steel which can transform during the welding thermal cycle [5–7].

Jointing of aluminum and steel is not a straightforward task, as the materials exhibit different melting points, different thermal diffusivities, different plastic work resistances, different surface oxides and different chemical affinity. Fusion techniques are capable of creating large Fe–Al reaction zones, strong distortion effects and defects associated with the solidification process. Mechanical jointing and adhesive bonding remain relevant, although they might require additional mass and surface treatment and might pose galvanic stability issues. Friction-based jointing presents an interesting opportunity, as it can involve minimal heating while preserving the ability to activate metallurgical bonds and avoid undesirable Fe-Al reactions [8,9].

Rotation speed is known to affect the welding process, because higher speed increases the sliding velocity, increases plastic deformation near the contact and therefore decreases the force necessary to drive the pin into the lap joint in position-controlled mode. However, the speed also has an influence on other aspects of welding, including duration of contact with elevated temperature, extent of heated aluminum and upward displacement of the steel substrate. The effect of rotation speed therefore becomes complex, since a process parameter which can be favorable from the viewpoint of machine control might be unfavorable from the viewpoint of interface chemistry and bonding structure [10,12**?**].

Friction stir spot welding is a technique which involves a localized version of friction stir welding, where a pin and shoulder rotate and penetrate into a lap joint formed of two sheets. As the pin and shoulder descend into the joint, plastic deformation of the upper sheet, interface disturbance and forging of a joint occurs during a relatively short dwell period. The fundamental reviews devoted to friction stir welding indicate that such processes are influenced by multiple factors, namely heat, plastic deformation, shoulder and pin design and cooling [13]. While friction stir spot welding does not include translational movement of the tool along the sheets, the annular flow pattern created by the rotating shoulder is particularly important. The rotating shoulder creates the conditions for upward steel displacement, aluminum flow and local exposure of the interface.

Multiple studies performed on aluminum/aluminum and dissimilar joints have confirmed that the key factors responsible for formation of the hook shape, bond width, amount of stirred material and joint strength are the dwell time, shoulder contact, tool design, penetration depth and rotation speed [14–19]. In refill-free spot welding, the exit hole and its surroundings play a particularly important role, as they represent the location where the loads acting on the joint are distributed during loading. While the bond itself is usually treated as an adhesive-like zone of uniform width and depth, the actual joint can be considered as a multi-layer structure which includes aluminum stirring zone, steel hooks, locally bonded annular region and chemically-reacted zone.

In addition to plastic flow of aluminum and upward displacement of steel, the interaction between aluminum and steel surfaces creates a chemical aspect of friction stir spot

welding. Formation of metallurgical bonds requires intimate contact and activation of the interface. At the same time, Fe-Al compounds are known to form spontaneously during friction stir spot welding due to high temperatures and pressures involved in the process. Studies conducted on Al-steel friction stir spot welding joints indicated formation of $FeAl_3$, Fe_2Al_5, $FeAl_2$ and similar intermetallic products with a morphology that depended greatly on speed, penetration depth and dwell time [20–24]. While thin and sparse intermetallic compound products can act as metallurgically-activated interfaces, high hardness and brittleness of these phases is likely to play a crucial role in the joint integrity.

A crucial element for characterizing the intermetallic compound distribution is the macrosection, because without the latter information, the chemical map would only reveal whether Fe-Al compounds are formed or not. On the other hand, without the presence of chemical data, the macrosections cannot provide any information about the exact nature of metallurgical bonds created. In particular, a hook rising above the surrounding surface and creating a point of concentration of loads is likely to contain intermetallic compounds and therefore serve as crack initiation site. The importance of combining macrosection with chemical analysis was demonstrated by previous works on FSSW joints [25].

The joint hook plays a crucial role during mechanical testing of lap joints as well, since it can provide mechanical interlocking and increase local contact area. At the same time, an overly high or sharp hook might behave like a stress concentrator for tensile forces and therefore decrease the strength of a friction stir spot weld. This means that evaluation of the joint width alone might be misleading if the associated hook and steel-side microstructure are not taken into account. As was already pointed out, earlier studies on aluminum/aluminum and dissimilar FSSW joints suggested coupling the assessment of hook shape with bond width [26–30].

The current study involves a joint of Al and dual-phase steel, which means that the steel is not only a substrate to be plasticized by the pin and shoulder but also a source of transformation during friction stir spot welding. Dual-phase steels rely on microstructure involving ferrite matrix and embedded martensite islands. Variations in martensite fraction, austenitization, carbon enrichment and ferrite continuity modify the initial microstructure and therefore modify initial hardness and behavior during welding. During FSSW, the underlying steel will undergo deformation, austenitization, quenching, tempering and transformation, depending on its location relative to the interface. Hardness profiling will therefore reflect both the initial heat-treated condition and thermal cycle during the process.

The two intercritical heat treatment conditions applied to the steel will allow to compare how the steel microstructure and hardness profile change with respect to each other. Heat treatment at 725 °C followed by water quenching will leave steel with relatively low martensite volume fraction. Heat treatment at 775 °C prior to quenching will result in increased fraction of austenite and therefore increased fraction of martensite in the final product. Such a significant difference in hardness, 327 HV vs. 377 HV for IHT725 and IHT775, respectively, allows evaluating the influence of material hardness on joint integrity. However, a difference of that magnitude will not separate the steel completely from the aluminum alloy, as both materials belong to a specific class of alloys.

The question being asked is not whether AA5754-H111 and Strenx 960 can be joined successfully. The more interesting question concerns how different combinations of rotation speed and steel hardness will distribute the benefits and drawbacks among the discussed phenomena, namely low process load, adequate joint width, proper hook formation, limited steel-side transformation and minimal Fe-Al reaction. Higher speed and higher hardness will lead to reduced force, enhanced interface activation, enlarged reaction zones and possibly altered hook geometry. The objective of the study is to evaluate which combination of parameters will result in optimal welding process for production of aluminum/steel spot welds.

The current paper relies on AA5754-H111/Strenx 960 lap coupons welded at rotation speeds of 800, 1200 and 2000 rpm after applying the two heat treatment procedures. It combines machine control data, optical macrosections, quantified hooks and bonded

widths, microstructure on steel side, hardness profiling and SEM-EDS images. The main contribution consists of interpreting aluminum/steel spot welds as a process-structure couple, where a parameter favorable for one outcome might be disadvantageous for others.

1.1. Materials and Experimental Setup

The welds were made from AA5754-H111 aluminum sheets with a thickness of 2 ± 0.2 mm and low-carbon Strenx 960 steel sheets with a thickness of 3 mm. The coupon geometry was square, sized 30 mm $\times$ 30 mm, and arranged in lap joints such that the aluminum sheet was located above the steel sheet. The order of sheets was chosen to ensure the pin rotates through the lower melting point aluminum before entering the stronger steel substrate. The welding process was done using an I-STIR PDS 4 system with position control. The tilt angle of the tool was fixed at 0° in order to eliminate the influence of tilt angle while analyzing effects due to different rotation speeds.

A composite tool design was applied. Specifically, the pin was a cylindrical WC–Co alloy with a nominal diameter of 4 mm, flat tip with dimensions of 3 mm $\times$ 3 mm, and a length of 2.4 mm. The shoulder was designed as a flat M42 steel alloy with a diameter of 12 mm. The plunge rate was kept constant at 12 mm/min, dwell time – 3 sec, and steel penetration depth – 0.7 mm. Rotation speed served as a varied parameter, which was set at 800, 1200, and 2000 rpm. Three trials were conducted for each case for metallography and hardness testing. Each test case was conducted three times for microstructural analysis and hardness testing. The constant plunge depth and dwell period ensured that the variations in load, hook size, width of steel transformed, and intensity of intermetallics could be attributed largely to rotational speed and the ratio of ferrite and martensite in the steel.

The process photographs and refined stack view in Figure 1 set the mechanical constraints for the following analysis. The fast dwelling period and controlled 0.7 mm steel insertion yield the small window where the steel pin has to produce sufficient interface interaction without overheating the interface itself. Considering the relatively large shoulder of 12 mm compared to the pin diameter of 4 mm, the heat generation and forging actions are assumed not only at the pin's periphery but also in the ring beneath the shoulder. Such geometric conditions explain why the bonding width and hooks' shape depend on the rotation rate despite constant plunging depth.

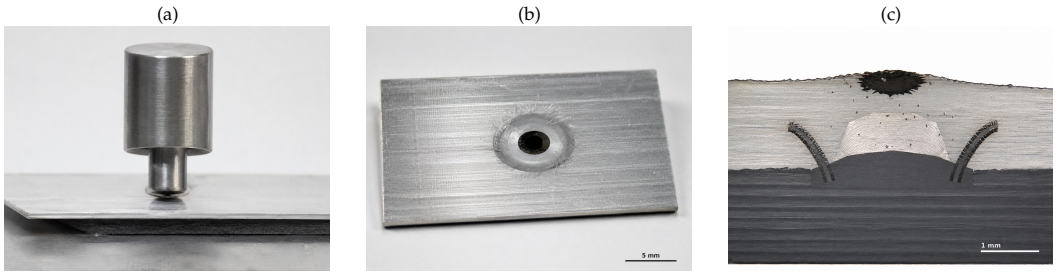

Figure 1. Process boundary and welded stack.

For intercritical heat treatment (IHT) before the welding, the steel sheets were exposed to the temperature in which two microstructures developed, depending on duration. First, dilatometry and subsequent calculations by Thermo-Calc software identified the intercritical range. Next, the steel sheets were kept at the temperature of 725 °C or 775 °C for 30 min each case and subsequently water quenched. Thus, the steel treated at 725 °C yielded lower martensite structure named IHT725 with martensite volume fraction of 0.38 and initial hardness of 327 HV. On the contrary, the structure with volume fraction of martensite of 0.61 and initial hardness of 377 HV was produced upon heat treatment of 775 °C. These two microstructures allowed examining whether the state of the steel influences weld development, either mechanically or metallurgically.

To investigate microstructural characteristics of welding, cross sections were taken with a metallographic preparation. Nital etch allowed revealing steel microstructure and distinguishing transformed steel and non-transformed steel zones. For optical microscopy

investigations, the exit hole, its morphology, hooks and bonded ring were analyzed. SEM and EDX were applied for analysis of the reaction layers at the tips of the hooks, vicinity to exit hole and the corners of the exit holes. Microhardness profiles were done on the surface of the exit hole with measurements down to the base steel to trace the transformation in stir zone, TMAZ, and HAZ and finally reach the undeformed base steel. Additional microhardness readings were conducted on intermetallics when possible due to their dimensions.

It is seen from the data presented in Table 1 that the experiment allows for distinguishing two different variables: on the one hand, the rotation speed determines the frictional power and consequently the plastic-flow regime; on the other hand, the two conditions of IHT differ in the initial phase composition of the steel. This is essential since the hardness difference alone does not explain the process behavior. The low-martensite steel may flow and flatten differently in the course of intensive heating; in the case of the high-martensite material, the deformation may be suppressed until thermal softening takes place and leads to a phase transformation. The described experiment structure hence enables determining how the initial microstructure translates into the resulting weld configuration.

Table 1. Materials and welding parameters.

Parameter	Experimental condition
Upper sheet	AA5754-H111, 2 ± 0.2 mm
Lower sheet	Strenx 960 low-carbon dual-phase steel, 3 mm
Coupon geometry	30 mm × 30 mm lap coupons with aluminum above steel
Steel treatments	725 °C for 30 min + water quench; 775 °C for 30 min + water quench
Initial steel state	IHT725: $V_m = 0.38$, 327 HV; IHT775: $V_m = 0.61$, 377 HV
Tool	WC–Co cylindrical pin, 4 mm diameter, 3 mm flat contact area, 2.4 mm length; 12 mm flat M42 steel shoulder
Process constants	0° tilt, 12 mm/min plunge rate, 3 s dwell, 0.7 mm steel penetration
Rotation speeds	800, 1200, and 2000 rpm
Replicates	Three welds per condition for metallography and hardness measurements
Characterization	Optical microscopy, SEM, EDS mapping, line scanning, point analysis, and microhardness profiling

In order to make the characterization process consistent, it was decided to perform the measurements in accordance with the physical evolution of a spot weld. The force-time measurements were done first as they allowed for recording the resistance to the plunge, then macrographs showed the final shape of the flow, the microstructural measurements revealed the transformation mechanism of the lower steel, the hardness profiling results correlated the structural changes with their mechanical consequences, and finally, SEM/EDS analysis made it possible to locate the chemical reactions around the dissimilar interface. It is significant since none of the tests conducted separately could have been used to describe an aluminum-steel spot weld completely: a low-force graph indicates valuable softening, but it says nothing about the bond width or intermetallic cracking. Similarly, a large bond observed with optical microscopy might hide an intermetallic crack in its corner exit zone.

2. Results and Discussion

2.1. Steel's initial microstructure and importance of joining process

The results of the intercritical heat treatments showed two different states of the microstructure in the steel. The steel in IHT725 had a greater fraction of ferrite, while the steel in IHT775 had an austenite content of 0.61, indicating presence of dense martensitic constituents. The hardness tests performed on both types of steel yielded values of 327 and 377 HV. This shows that there was an increase in the fraction of austenite content prior to the quenching process, leading to formation of increased amount of martensite in the final microstructure. Metallurgically, the difference implies that the fraction of ferrite would facilitate easy plastic accommodation, while the amount of martensite will increase the steel's local strength as well as how the steel reacts to the upward displacement created by the tool.

As a result of these two different microstructures, there would be two ways of accommodating the joining process. For the sample IHT725 with a higher fraction of ferrite, more continuous plastic deformation is expected prior to austenite transformation through

heating of the contact layer. In this case, the process of lateral spreading can be facilitated after the interface reaches adequate level of heating and compression. In case of the IHT775 sample, the greater martensite content implies increased initial resistance, making more localized upward reaction possible before softening occurs through heating. This difference is unlikely to be observed in terms of applied force but in final hook height, width, and bond width after removal of the tool.

The micrograph images and hardness impression image shown in Figure 2 set the state of reference for understanding the behavior of the welds on the steel side. The ferrite phase appears more distinct in IHT725, whereas the IHT775 grade shows more continuity of the dark martensite phase in its microstructure. These differences have an effect during friction-stir-welding (FSSW). The lower sheet undergoes heating with a temperature and strain gradient. An increase in the amount of ferrite makes the structure more deformable in the direction transverse to the travel of the tool once heated, while more martensite can cause more drastic upward motion once it contacts the softened aluminum alloy. The following analysis shows that the difference between the materials manifests in the force signal, but even more significantly in the hook and bond geometry.

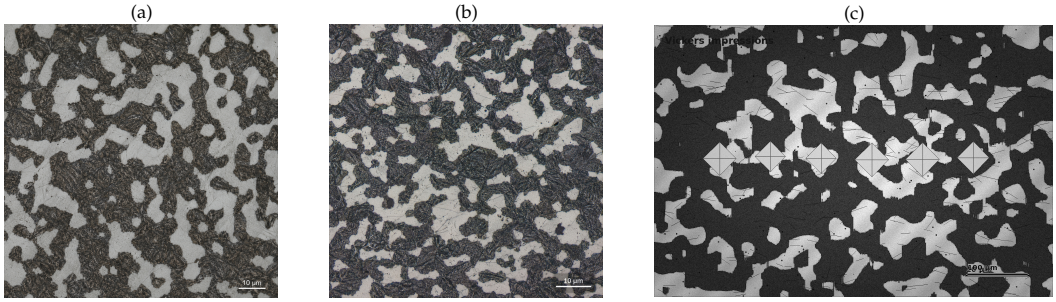

Figure 2. Initial steel states.

The hardness difference between the materials can serve to distinguish the strengthening prior to the welding operation from any possible transformation that occurs during welding. Although a higher initial hardness in the IHT775 does not necessarily mean a hard stir zone due to the possibility of reaustenitization and transformation of the near-surface layers of the steel, a low hardness of the IHT725 grade does not mean the lack of transformation due to high temperature and strain near the tool pin. In other words, what is important is the amount of steel that experiences transformation into an austenitic state during welding. Indeed, the mechanical response of dual-phase steels depends on phase distribution and thermal history and not on nominal hardness alone [31–33].

2.2. Plunging-force response and thermal softening

As is seen from the plunging-force traces in Figure 3, the process resistance to the plunge varies as a function of rotation speed. At the lowest value of rotation speed, the tool faces the highest resistance while it plunges into the aluminum alloy and touches the steel. By increasing the rotation speed to 1200 rpm, the force decreased; the force reached its minimum value at 2000 rpm. For both types of steel studied, the same trend was observed, and it was caused by the heat generation and thermal softening of the workpieces. It is apparent from the traces in Figure 3 that plunging force exhibits time-dependent loading-unloading pattern.

As can be seen from Figure 3, rotation speed has a much greater impact on process force than initial ferrite-to-martensite distribution in steel. For a given rotation speed, the difference between IHT725 and IHT775 is negligible compared to the effect of increased speed on process force. Intuitively, it makes sense because the tool first heats and plasticizes the aluminum, and then drives the steel surface into a highly strained, high-temperature state. At such state, the resistance becomes increasingly dependent on the thermal state of the steel induced by rotating tool, not its hardness difference at room temperature (327 vs. 377 HV).

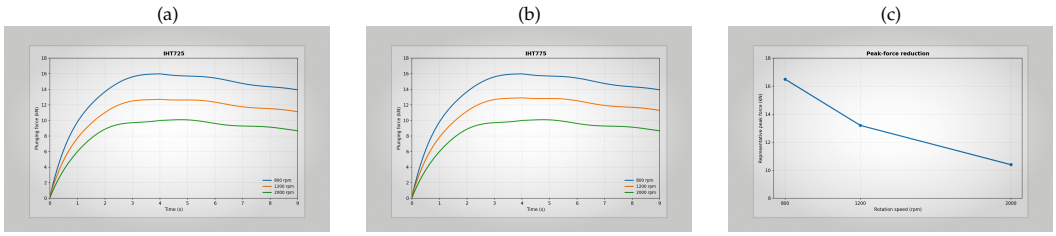

Figure 3. Plunging-force response.

In terms of actual force peak value, low speed corresponds to 16.5 kN of force, which drops down to 13.2 kN at the intermediate speed and 10.4 kN at the highest speed. Such decrease in force can be relevant to process stability, machine requirements, tool life, and repeatability of cycle. In addition, it shows that rotation speed is not just a kinematic parameter but a thermal control one as well. Since the plunge depth remains the same for all three cases, the lower forces imply less deformation resistance in both materials at higher speed. Consistent with FSW principles, heat generation and flow stress govern the plunging resistance.

Thus, from a practical point of view, higher rotation speed means lower loading of the tool and better process performance. It would mean less stress imposed on the spindle, fixture, and backing plate in the welding machine. However, force measurement can never provide sufficient information on joint integrity and quality. While higher thermal input can reduce plunging resistance, it simultaneously leads to a broader steel transformation and enhanced interfacial chemical reaction. In other words, the measurement of force serves as an early indication of material softening but needs to be considered in relation to the cross-section analysis of hooks, bonds, and Fe-Al reaction layer.

An explanation for decreased plunging resistance lies in the heat generation properties of FSW process. Higher rotation speed increases relative deformation rate of aluminum and results in higher temperatures and lower flow stress in the vicinity of tool elements. Because the process is position-controlled, the effect takes place mostly via lowering the loads. As noted previously in literature, FSW process depends on heat generation, heat transfer, and material flow [10,12]. In this regard, the presented welding process demonstrates the highest energy input combined with the lowest process loads. It produces the most pronounced effects on interfacial transformations.

Finally, it is interesting to observe the moderate influence of initial steel hardness (50 HV difference) on plunging force. Clearly, the difference is visible before the welding process, but it does not result in similar distinction in the peak force values during plunging. Thus, the resistance of steel to plunging occurs mostly due to local thermal state, not due to steel hardness at room temperature. This way, any force measurement system would allow for detection of insufficient or excessive rotation speed but not for determination of starting martensite fraction. Therefore, the force trace is a thermal-softening indicator, while metallography characterizes transformation.

2.3. Cross-sectional morphology and material-flow path

The cross sections show how the flow of materials induced by FSW process translates into joint geometry. Every weld contains an exit hole made by the pin, deformation of the steel along the outer edge of the pin, and annular bonded zone between aluminum and steel. The bottom sheet was not left flat – it was bent and formed into hooks as a sign of pronounced local strain and deformation. The weld morphology changes as a function of rotation speed and initial steel condition.

From the cross sections shown in Figure 4, it can be observed that the welding zone needs to be considered as an asymmetric three-dimensional flow product and not as a symmetric spot. In this regard, the hook reflects the effect of upward movement of the steel, while the bonded zone represents the width of the zone of interfacial interaction and its activation underneath the aluminum plate. Under a low rotation rate of 800 rpm, there was no significant difference in the hook heights, which implies that the lower thermal energy

did not significantly influence the ability of the microstructure to change the deformation path. On increasing speed, there was some difference in morphology of the two steel conditions, where the hook height was greater in IHT775, but the bond-width expansion was prominent in IHT725.

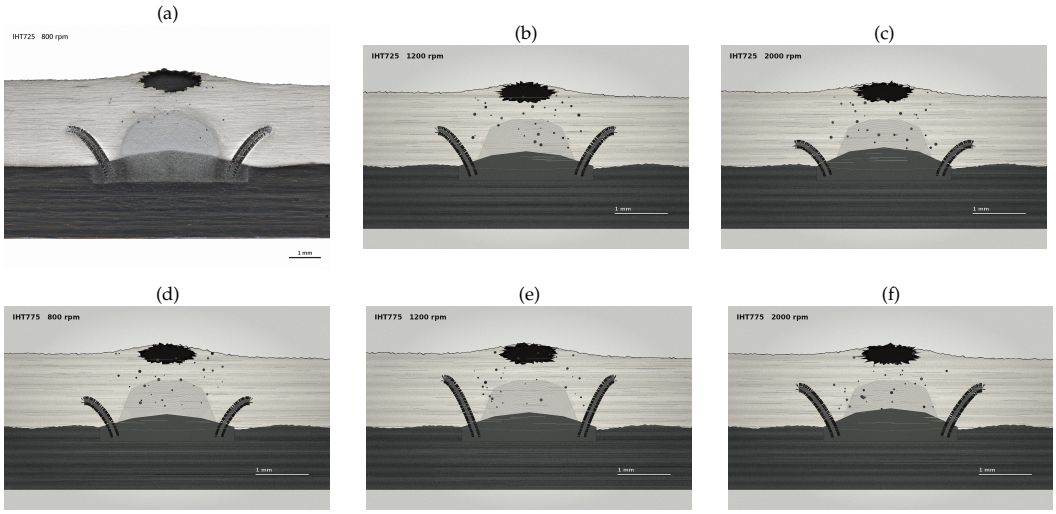

Figure 4. Speed-ordered weld sections.

From the morphology, the geometry shows that the rotation rate influences the ratio of vertical deformation to lateral spreading. Under a low speed condition, thermal energy is too weak to induce sufficient plasticity for both. However, when rotation increases, thermal softening of the material around the pin and shoulder occurs such that both vertical deformation and lateral movement become feasible. It appears that the steel with a high amount of martensite is favorable for producing a high hook under high-energy conditions, while the steel with a relatively low level of martensite produces a large bonded zone.

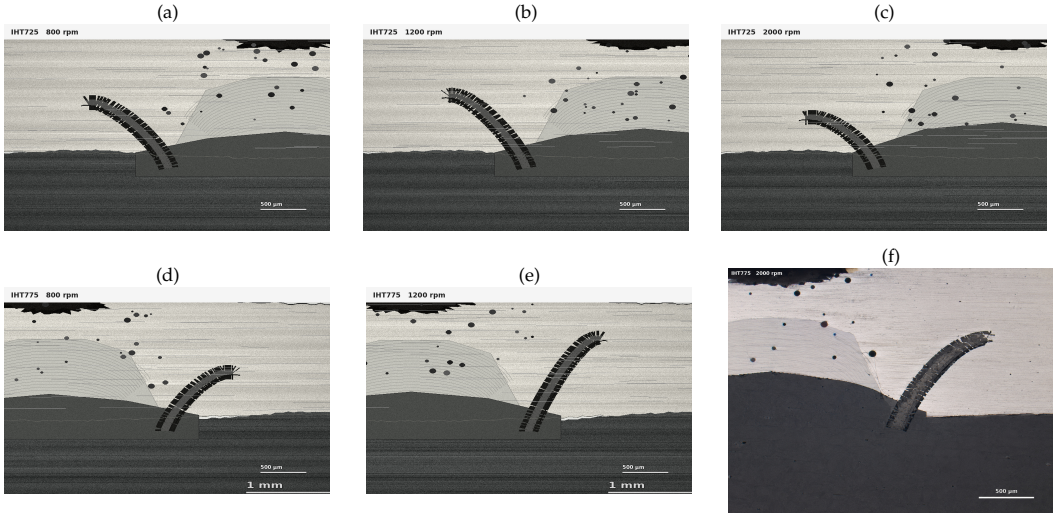

Figure 5. Hook and bond close views.

Panels within the insets in Figure 5 provide an indication of hook and bond geometry, thus establishing the trade-off geometry. Hook height of the IHT725 case is approximately 900 μm at 800 rpm, grows slightly at about 1200 rpm and reduces to approximately 740 μm at 2000 rpm. The corresponding value for IHT775 is slightly smaller at 800 rpm, grows rapidly up to about 1200 μm at 1200 rpm, and is larger than IHT725 again at 2000 rpm. As concerns the hook width, IHT725 exhibits a relatively large hook at 800 and 1200 rpm,

while IHT775 becomes the condition with wider hook at 2000 rpm. The bond width is a critical parameter since it determines the load transfer ability. Thus, this parameter changes insignificantly between 800 and 1200 rpm and then grows significantly at 2000 rpm. For the first case it reaches about 850 μm, while for the second case it reaches only about 725 μm. These results demonstrate that bond enlargement is not necessarily a continuous linear effect; it emerges once the thermal-mechanical loading is intense enough to promote lateral interfacial interaction.

A comparative evaluation of the three parameters shows that neither hook nor bond is characterized by a simple monotonic dependence of any welding parameter. Thus, the highest speed condition with IHT725 produces the largest bond size but not the largest hook height, while the intermediate speed IHT775 condition creates the highest hook without creating the largest bonded width. This behavior is meaningful from the physical perspective since the vertical growth of hook means steel lifting, while the growth of bond implies lateral activation and intimate contact along the interface. Thus, both effects can be stimulated by heating and deformation, but they need not change concurrently. This result is particularly important for engineering applications since a specification based solely on hook height might be inclined towards selecting a condition with sharper notch, while the specification based only on bonded width would ignore local reaction products. Hence, for accurate evaluation one should consider both dimensional measurements and interfacial microstructure.

As far as the dimensions obtained are concerned, they have to be interpreted with great care. Thus, a greater height of the hook does not necessarily mean an improvement since the hook tip itself represents a notch potentially capable of bearing brittle intermetallics. A large bonded width is desirable since it enlarges the bonding surface and provides a greater load transfer potential. However, it may be associated with greater Fe–Al reaction development. Similarly, a large hook width might be considered positively when placed outside the bonded ligament since it indicates enhanced interlocking potential. On the other hand, it may be a consequence of steel excess transport. Therefore, the best morphology will not be represented by a single dimension. It will be defined by sufficient bonded area and proper hook shape without stress concentration or brittle intermetallic placement in the stressed area.

It should be noted that the behavior of IHT725 and IHT775 cases at 2000 rpm is highly indicative for understanding the process specifics. As far as bonding is concerned, the steel case with lower martensite content gives a broader bond, which implies higher lateral stimulation of the Al-steel interaction in spite of higher rotational speed. The steel with higher martensite content gives more prominent hook, which can be advantageous for enhancing mechanical interlocking; however, it can also imply increased sensitivity to notching and brittle behavior. This behavior explains the inability to rely solely on the force signal even in the cases of small differences between two steels. The force signal represents the momentary material softening, while the cross-sectional structure represents the total material flow history.

2.4. Transformation of steel at the exit hole location

The region below the exit hole did not experience merely plastic deformation. Steel transformation took place. Thus, the steel directly beneath the tool surface became completely martensitic due to exposure to austenitization conditions and fast cooling. Further down the metal, the microstructure gradient showed that this transformation continued through the thermomechanically affected zone and heat-affected zone before the ferrite–martensite structure of the base steel was restored.

The etched transformation fields described in Figure 6 explain the origin of geometrical and hardness characteristics. Immediately underneath the stirring pin tip, the original microstructure of IHT725 or IHT775 is replaced by the martensitic structure emerging due to the high-temperature and high-deformation state of steel. Moving further away from the top sheet's contact, the presence of the original microstructure becomes increasingly

apparent, because the temperatures and deformations are relatively low there. In addition, the difference in geometry of hooks allows us to conclude that the original microstructures of the two steels are partially preserved in the deeper parts of the joint, which leads to a variation in hardness behavior.

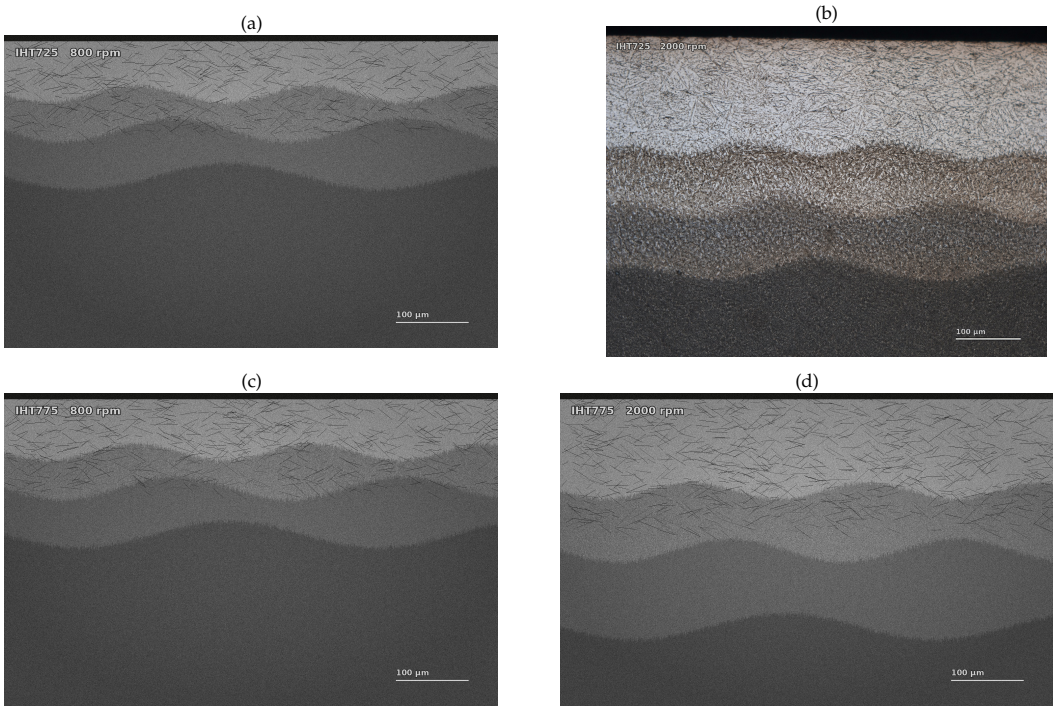

Figure 6. Steel transformation beneath the exit hole.

An increase in rotation speed enlarges the transformed steel region. This phenomenon stems from the same thermal softening mechanism responsible for the reduced plunging force. The higher rotation speed provides more frictional and deformation heating, resulting in transformation of a larger portion of steel at the interface between sheets. On the one hand, the effect benefits the formation of bonds by enabling additional thermal activation necessary for plastic material flow. On the other hand, a larger area of transformed steel can lead to an increased hardness gradient, as well as to a growth in brittle phases and residual stresses that could affect the cracking resistance. Friction stir spot welding studies of high-strength steels also reveal that local transformation in the vicinity of the tool controls the mechanical response despite the small size of the macroscopic joint [34–37].

The microstructural zoning of the welded material can also explain the significance of dwell time and penetration depth, although both parameters were held constant. The 3-second dwell time is rather short, but sufficient for achieving severe thermomechanical conditions within the area of direct contact with the tool. In addition, the 0.7 mm penetration of the lower sheet means that not only the top surface is thermomechanically affected, but a direct interaction between the lower sheet and tool takes place. Therefore, such dwell time and penetration depth guarantee transformation of the steel into a martensitic layer with an adjacent region of mechanical disturbance and heat-affected zones. Thus, the observed hardness gradient can be attributed to a carefully managed but intense local process, and not melting or bulk fusion.

In addition, the transformed zone allows explaining why the weld cannot be considered solely on the side of aluminum. Despite being the upper and lower-melting metal in this configuration, the 0.7 mm penetration into the steel makes it also a part of the weld, actively involved in the process. The mechanical disturbance at the top surface, emergence of a layer of high temperature, and subsequent fast cooling upon tool withdrawal can result in a local martensitic transformation followed by transition to partially affected and unaffected regions. Hence, the local gradient emerges on the steel side and can influence stress

distribution in the joint under load. Similarly to friction stir spot welding of high-strength steels, a local steel-side transformation was found to dominate the mechanical behavior of the weld.

2.5. Hardness profile and mechanical implications

The depth-dependent microhardness profiles reflect the previously discussed microstructural zoning, beginning at the surface of the exit hole and continuing into the lower sheet. The largest microhardness value is observed in the region immediately underneath the stir pin, corresponding to the martensitic structure of the stir zone. Further away from the surface, microhardness gradually drops down to the initial level of IHT725 or IHT775 steel.

It can easily be seen from the Figures 7, however, that the hardness is highly dependent on depth, so that a single number cannot represent the condition of the weld. Near the exit-hole surface, there is transformation-related hardening due to martensite. Deeper into the material, the competition between partial transformation, tempering of existing martensite, and the influence of deformation takes place. At larger depths, the measured hardness levels approach those of the original steel again. As such, the contrast between IHT725 and IHT775 increases as well, indicating that the final gradient is formed by hardening and softening mechanisms simultaneously. This result is in agreement with literature about steel friction processing [38–41].

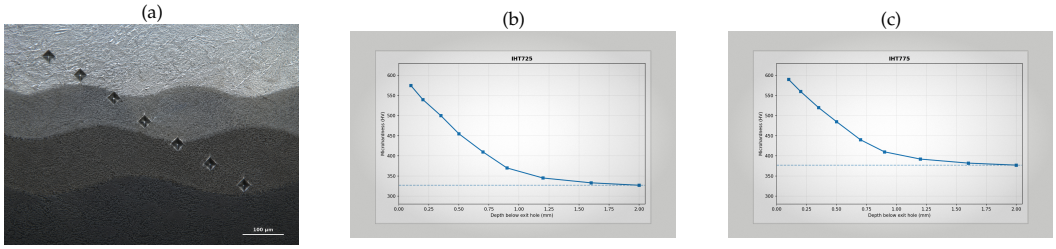

Figure 7. Steel hardness gradient.

In terms of profile shape, the existence of a homogeneous hard layer of constant thickness is not found in this experiment, either. Hardness starts out relatively high near the exit-hole surface, drops through the transition regions, and finally approaches the hardness of the base steel. In IHT725, the relative increase due to transformation effects is especially noticeable due to the lower hardness of the initial microstructure. For IHT775, the contrast to the base hardness level is relatively low due to the increased starting hardness, although the initial microstructure near the exit hole is highly martensitic. In any case, hardness must be viewed relative to the phase structure present before processing, not independently of the history of heat treatments.

Structurally, the hardness gradient becomes relevant due to the possibility of local crack initiation. While the presence of a hard layer may lead to better mechanical resistance, it may equally reduce overall ductility in a complicated area. At the same time, a softer transition layer may offer flexibility while becoming preferred for deformation if peel and bending tests are performed. In this case, the combination of a hard surface layer, softer subsurface region, hook curvature, and intermetallic particle is more valuable than just the hardness itself.

The profile shape being nearly identical between IHT725 and IHT775 is another piece of supporting information that helps conclude that only the force response curve shows a clear difference between samples. As such, the welding cycle dictates the severity of the process at the bottom of the indenter while the starting microstructure influences the depth at which the steel reaches its initial conditions. From a production point of view, this means that measuring only the hardness near the exit hole does not allow for a fair comparison of different incoming materials, since the full gradient should be considered, as well as the final geometry.

2.6. Fe–Al intermetallic reaction and local brittleness

The products of reaction between iron and aluminum were detected near the tips of hooks, on the edges of hooks in the proximity of the exit hole, and at the exit-hole corners. These areas correspond to the most vulnerable locations due to the combined effect of high contact pressure, deformation, temperature, and geometric stress concentration. Based on SEM contrast and EDS spectra, there was an indication of Fe and Al existing in the reaction products together. Also, at least two types of Fe–Al alloy were detected using point analyses [42].

The results of the SEM, EDS, and line-scan panels presented in Figure 8 demonstrate that intermetallic formation in the welding seam occurs locally rather than uniformly along the interface. This distinction is key. While a small discontinuous reaction layer at the properly supported interface does not necessarily drive failure, a hardened and cracked reaction layer at the exit-hole corner can act as a site of damage initiation. The obtained hardness range of 456–937 $HV_{0.1}$ is significantly higher than that of both base materials and the region of transformed steel. The direct observation of the cracks within the intermetallic zone confirms that the reaction layers exhibit a brittle behavior.

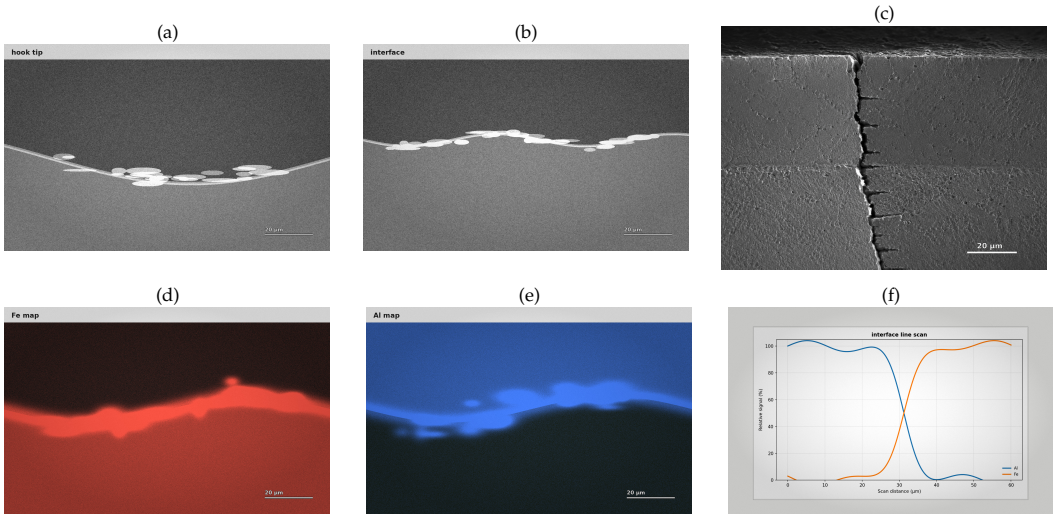

Figure 8. Fe–Al reaction sites.

The presence of cracks within the intermetallic layers at the exit-hole corner shows the most critical aspect of all the examined joints. The corner itself represents a geometric discontinuity created by the retracting pin, while adding a highly hard Fe-Al constituent into this region adds a material discontinuity. Such combination of features will easily concentrate stress even if the whole joint is subjected to shear load in service. Hence, the high hardness range of 456–937 $HV_{0.1}$ has a mechanical meaning — the hardness of the constituents in question is several times higher than the hardness of the base materials and is not likely to allow any plastic deformation to occur. Thus, the intermetallic results put the metallurgical limit to benefits of higher rotation speeds.

The location of the observed phases explains the main drawback associated with increased rotation speed. With the 2000 rpm speed, the width of the bond gets larger, in particular in the case of IHT725. The same intensification of the process, however, leads to stronger formation of Fe-Al reaction products. Hence, there is a trade-off inherent to this process — too little power will lead to weak bonding and low activated annulus, whereas too much energy will increase the risk of formation of intermetallics in the critical region where local stresses are the highest due to curvature and exit hole. Therefore, the appropriate window of rotation speed needs to be chosen according to the available data regarding bond width, hook shape, hardness gradient, and cracking of intermetallics.

The hardness values of intermetallics explain why chemistry cannot be neglected in favor of geometry. A bond formed in the joint can be viewed as continuous in the optical

image while being brittle and cracked if examined microscopically. Alternatively, even a joint exhibiting relatively small bond width can operate properly as long as the formed intermetallics remain thin and discontinuous at a safe distance from the stress concentrating sites. In the current example, high hardness of reaction products in the hook and exit hole vicinity makes the increased bond width achieved at 2000 rpm rotation speed undesirable. Similar conclusion was made for aluminum-steel spot and friction stir welds [20,21,23,25].

2.7. Combined process-window interpretation

All of these observations indicate that what occurs here is a coupled structure-process response. The speed of rotation controls the production of heat and also the lowering of the load. Faster rotation causes less plunging load and provides the lateral loading required to cause bonding. The starting microstructure of the steel does not affect the amount of force generated because this area is quickly heated up and made soft by the contact from the tool, but the starting microstructure of the steel has an influence on the morphology of the joint since it must be deformed, transformed, and then recovered during the process of forging the interface.

The pictures of the conditions shown in Figure 9 link the internal cross-section observations with the external manifestation of the welded regions. The series of six pictures allows interpreting the process window in terms of an array of similar results rather than individual examples. The conditions with 800 rpm show higher dominance of mechanical influence, while for the 2000 rpm conditions, the effects of heat are more pronounced along with flow around the tool. The photographs clearly demonstrate why appearance alone cannot be taken as the only criterion for acceptance. Even though the appearances at the top surface are alike, different depths of hooks, bond widths, transformed volumes of steel, and intermetallic reactions can be expected beneath the exit hole. Because of this, the process window analysis has to consider not only the surface result but also the results from the cross-sections and microstructure.

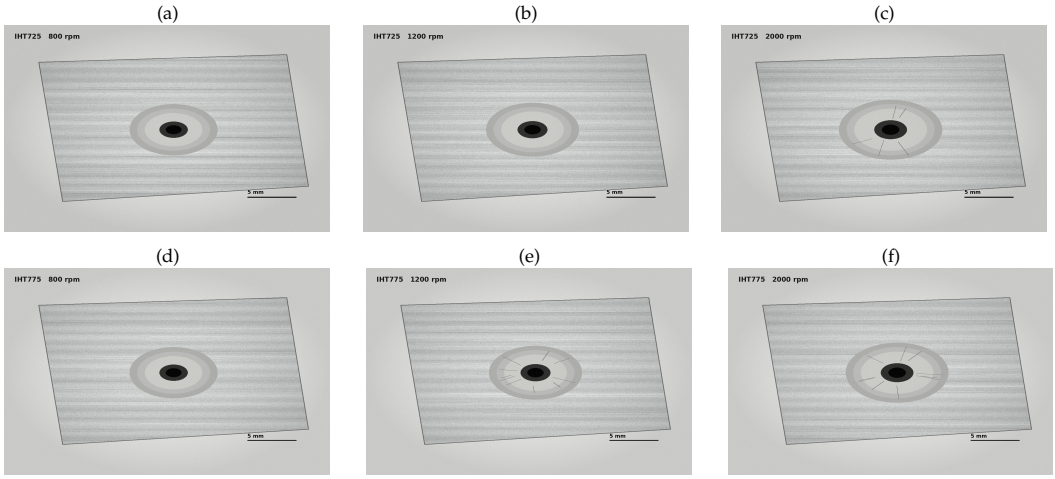

Figure 9. Condition-level surface outcomes.

Table 2. Main measured trends.

Descriptor	Observed response
IHT725 starting steel	Martensite volume fraction 0.38; initial hardness 327 HV
IHT775 starting steel	Martensite volume fraction 0.61; initial hardness 377 HV
Rotation-speed effect on force	Increasing speed from 800 to 2000 rpm reduced the peak plunging demand for both steel conditions
Microstructure effect on force	Small compared with the effect of rotation speed at a fixed plunge depth and dwell time
Hook height	Comparable at 800 rpm; larger for IHT775 at 1200 and 2000 rpm
Hook width	Larger for IHT725 at 800 and 1200 rpm; larger for IHT775 at 2000 rpm
Bond width	Limited change from 800 to 1200 rpm; clear increase at 2000 rpm, strongest for IHT725
Steel-side transformation	Fully martensitic stir zone beneath the exit hole, followed by TMAZ, HAZ, and return toward initial DP structure
Intermetallic locations	Hook tips, hooks near the exit-hole interface, and exit-hole corner
Intermetallic hardness and condition	456–937 $HV_{0.1}$; local cracking at the exit-hole corner

From Table 2, one sees why selection on the basis of any one parameter is inadequate to identify the optimal condition. Low plunge force means excellent softening of the aluminum, less energy dissipation into the machine, and less chance of tool chatter; however, it does not say anything regarding brittle intermetallic formation in the interfacial bond. Large bond width means good load-transfer capability; however, this may be due to an enhanced chemical reaction. High hook means increased mechanical interlocking; however, it means formation of notches. The presence of a hardened martensite layer means better contact; however, the hardness gradient is undesirable since it compromises ductility. Therefore, process optimization for AA5754-H111/DP-steel FSSW should not only focus on a single parameter such as minimum force or maximum bond width.

A good process window can be defined in terms of multiple outcomes. First, the force trace should be relatively low; that means sufficient softening of the alloy and tool stability. Second, the bond width should be sufficiently large; that means continuous load-transfer ability. Third, the hook should exist but be limited to avoid forming a notch. Fourth, there should be enough martensite transformation in the steel but limited hardness gradient to ensure contact without brittleness. Fifth, the Fe–Al intermetallics should be discontinuous and not prone to cracking at the exit-hole corners. From the matrix, it appears that 2000 rpm is the best option for force reduction and enlarged bond width. On top of that, IHT725 produces the largest bond width at this speed; thus, it is most suitable in case of bonding annulus optimization. Nonetheless, IHT725 still needs careful management since it promotes brittle Fe–Al reaction products.

In the considered matrix of processing parameters, 2000 rpm appears to be the most efficient rotation speed for reducing the process force and maximizing the annular bond width. In particular, IHT725 exhibits bond widening to its highest level among all other conditions. Thus, the lower martensite content of this grade is beneficial for obtaining good bond width. On the other hand, IHT725 needs to be handled with care because this condition enhances both the thermal and chemical reactivity for Fe–Al intermetallic formation. At the same time, the higher speed tends to produce more pronounced hooks in IHT775. This may indicate improved interlocking, but it also suggests concerns about notch generation and increased brittle reaction products at hook regions. Therefore, the optimum is not achieved merely by reaching high speed, but by maintaining it while controlling hook sharpness and brittle reaction products.

There are implications of the analysis in terms of how the incoming DP-steel should be characterized. If the steel martensite content is subject to variation, the same force curve may represent different amounts of intermetallic and/or hooks even if it is still in the desired range. Hence, force monitoring may be an unreliable means of quality control for the process. In addition to the weld geometry characterization (hook and bond width), metallographic validation of the process should cover at least the initial steel phases, hardness gradient, intermetallics in the bonds, and their tendency to cracking. When the above relationship becomes well-defined, the force curve may become a quick assessment parameter.

3. Industrial Significance

From an industrial perspective, the significance of this welding test lies in the close relationship between mechanical properties and metallurgical reactions that may compromise performance of the joint. For the production of lightweight vehicle structures, low force level and short cycle time are positive attributes only in those instances in which the joint retains stable internal microstructure. In the current case, higher rotation rate decreases the load while improving bond development, and increases the strength of the interfacial reaction. These findings can be useful for the design of dissimilar sheet-assembly processes, in which aluminum-steel joints often experience mixed shear, peel, and bending stresses, which depend on local notch effect and brittle intermetallics.

Another lesson from the findings presented above is that mechanical testing alone is insufficient for process verification. On one hand, destructive lap-shear strength values can

rank individual specimens based on their mechanical characteristics. On the other hand, this measure does not allow determining whether load resistance stems from bond size, proper hook geometry, transformation of steel sheets, and lack of intermetallic formation. The current data suggest that all these properties can change independently of each other. A given weld specimen may exhibit low force trace, broad bond, but possess cracked intermetallic product located near critical corners. Thus, a reliable industrial procedure must combine mechanical testing with a set of metallographic indicators: initial hardness of the steel, geometry of the hook, bond size, hardness profile, and existence of a cracked intermetallic product.

At the same time, mechanical testing can never be considered as sufficient for process verification. A lap-shear test value can help ranking individual samples, but it will not provide information on what factors contribute to load resistance. The current study provides evidence that this contribution varies independently of each other. Even if a weld specimen exhibits relatively broad bond geometry, it may still contain a cracked intermetallic in the critical corner. Thus, the qualification procedure must include metallographically detectable properties besides mechanical testing. In this respect, force monitoring of every weld point and occasional cross-sectional examination of bond size, hook geometry, transformed steel thickness, and Fe–Al reaction products appears to be optimal. In particular, this procedure is consistent with the existing industry practices, which rely on force monitoring and cross-section evaluation.

It must be noted that the initial steel condition represents an important process variable, which should be taken into account in the qualification procedures. Typically, most efforts are directed at controlling tool wear, machine load, plunge depth, and surface state of the sheets. However, this study revealed that even without any substantial changes in these parameters, the proportion of ferrite and martensite in the lower sheet can produce dramatic changes in geometry of hooks and bonds, thus affecting the final weld characteristics. Therefore, the control of dissimilar FSSW process should include both verification of material states and machine parameters.

As a result, the suggested window of the FSSW process for joining AA5754-H111/DP-steel sheets should prefer the parameters that promote bond formation and minimize notches and cracks in the hook regions. The current data recommend using a high rotation rate to decrease load and promote bond formation, especially for the lower-martensite alloy. However, since the interfacial hardness measurements and microstructure analysis revealed cracks and high hardness peaks, the rotation rate optimization should proceed carefully. Force monitoring and cross-sectional evaluation of bond size and hook geometry seem to be appropriate measures.

4. Conclusions

Rotation speed and starting microstructure influence different characteristics of the AA5754-H111/DP-steel friction stir spot welding process. While rotation speed dominates the process load and thermal activity (decreasing plunging resistance from 800 to 2000 rpm), the lower sheet microstructure has a smaller impact on the force signal. Hence, maximum process force cannot provide insight into the way the bottom sheet deforms during friction stir spot welding.

Final bond geometry is the main distinguishing feature between the two initial states. While the higher-martensite steel (IHT775, 0.61 Vf and 377 HV) produces greater hooks during processing at 1200 and 2000 rpm, the lower-martensite one (IHT725, 0.38 Vf and 327 HV) produces optimal bond-width extension under 2000 rpm. Therefore, the key conclusion is that a condition characterized by less martensite content can favor lateral bond evolution during fast welding while high martensite content leads to the formation of larger hooks under sufficient energy input.

Steel below the exit hole experiences a genuine transformation series involving martensite production followed by the recovery of dual-phase structures. Microhardness profiles demonstrate that steel in this region is relatively hard close to the surface and gradually

softens to the initial value depending on the depth. The hardness distribution should thus be treated as a joint attribute because it affects local deformability and bonding quality as well as the interaction between the hook and interface.

Hard brittle Fe-Al intermetallic phases are the main weakness introduced to the bond under high-speed friction stir spot welding. These phases occur on the hook tips, near the interface at the exit hole, and in the exit-hole corner region. Hardness of 456-937 $HV_{0.1}$ combined with cracking observed in the latter region means that such products can become a source of structural defects despite any growth in bond width. Thus, the answer to the research question is limited to stating that high rotation speed is beneficial for reducing process forces and promoting bond formation, especially for IHT725, as long as proper hook geometry and intermetallic products occur. Reliable AA5754-H111/DP-steel friction stir spot welding can be achieved using the criteria based on the combination of process load, bond width, hook geometry, transformed steel width, hardness distribution, and intermetallic cracking. This two-in-one criterion emerges as the most plausible solution to the problem of process design because it captures all of the beneficial attributes of large rotational inputs without allowing any potential for local brittle fracture.

References

[1] Goede, M.; Stehlin, M.; Rafflenbeul, L.; Kopp, G.; Beeh, E. Super Light Car - lightweight construction thanks to a multi-material design and function integration. *European Transport Research Review* **2009**, *1*, 5–10.

[2] Meschut, G.; Janzen, V.; Olfermann, T. Innovative and highly productive joining technologies for multi-material lightweight car body structures. *Journal of Materials Engineering and Performance* **2014**, *23*, 1515–1523.

[3] Tisza, M.; Czinege, I. Comparative study of the application of steels and aluminium in lightweight production of automotive parts. *International Journal of Lightweight Materials and Manufacture* **2018**, *1*, 229–238.

[4] Karim, M.A.; Park, Y.D. A review on welding of dissimilar metals in car body manufacturing. *Journal of Welding and Joining* **2020**, *38*, 8–23.

[5] Shah, L.H.; Ishak, M. Review of research progress on aluminum-steel dissimilar welding. *Materials and Manufacturing Processes* **2014**, *29*, 928–933.

[6] Haghshenas, M.; Gerlich, A.P. Joining of automotive sheet materials by friction-based welding methods: A review. *Engineering Science and Technology, an International Journal* **2018**, *21*, 130–148.

[7] Shen, Z.; Ding, Y.; Gerlich, A.P. Advances in friction stir spot welding. *Critical Reviews in Solid State and Materials Sciences* **2020**, *45*, 457–534.

[8] Dilthey, U.; Stein, L. Multimaterial car body design: challenge for welding and joining. *Science and Technology of Welding and Joining* **2006**, *11*, 135–142.

[9] Tanaka, T.; Morishige, T.; Hirata, T. Comprehensive analysis of joint strength for dissimilar friction stir welds of mild steel to aluminum alloys. *Scripta Materialia* **2009**, *61*, 756–759.

[10] Mishra, R.S.; Ma, Z.Y. Friction stir welding and processing. *Materials Science and Engineering R: Reports* **2005**, *50*, 1–78.

[11] Nandan, R.; DebRoy, T.; Bhadeshia, H.K.D.H. Recent advances in friction-stir welding - process, weldment structure and properties. *Progress in Materials Science* **2008**, *53*, 980–1023.

[12] Jedrasiak, P.; Shercliff, H.R.; Reilly, A.; McShane, G.J.; Chen, Y.C.; Wang, L.; Robson, J.; Prangnell, P. Thermal modeling of Al-Al and Al-steel friction stir spot welding. *Journal of Materials Engineering and Performance* **2016**, *25*, 4089–4098.

[13] Threadgill, P.L.; Leonard, A.J.; Shercliff, H.R.; Withers, P.J. Friction stir welding of aluminium alloys. *International Materials Reviews* **2009**, *54*, 49–93.

[14] Su, P.; Gerlich, A.; North, T.H.; Bendzsak, G.J. Material flow during friction stir spot welding. *Science and Technology of Welding and Joining* **2006**, *11*, 61–71.

[15] Lathabai, S.; Painter, M.J.; Cantin, G.M.D.; Tyagi, V.K. Friction spot joining of an extruded Al-Mg-Si alloy. *Scripta Materialia* **2006**, *55*, 899–902.

[16] Tozaki, Y.; Uematsu, Y.; Tokaji, K. Effect of processing parameters on static strength of dissimilar friction stir spot welds between different aluminium alloys. *Fatigue and Fracture of Engineering Materials and Structures* **2007**, *30*, 143–148.

[17] Fujimoto, M.; Koga, S.; Abe, N.; Sato, Y.S.; Kokawa, H. Analysis of plastic flow of the Al alloy joint produced by friction stir spot welding. *Welding International* **2009**, *23*, 589–596.

[18] Yang, Q.; Mironov, S.; Sato, Y.S.; Okamoto, K. Material flow during friction stir spot welding. *Materials Science and Engineering A* **2010**, *527*, 4389–4398.

[19] Shen, Z.; Yang, X.; Yang, S.; Zhang, Z.; Yin, Y. Microstructure and mechanical properties of friction spot welded 6061-T4 aluminum alloy. *Materials and Design* **2014**, *54*, 766–778.

[20] Figner, G.; Vallant, R.; Weinberger, T.; Enzinger, N.; Schröttner, H.; Pašič, H. Friction stir spot welds between aluminium and steel automotive sheets: influence of welding parameters on mechanical properties and microstructure. *Welding in the World* **2009**, *53*, R13–R23.

[21] Bozzi, S.; Helbert-Etter, A.L.; Baudin, T.; Criqui, B.; Kerbiguet, J.G. Intermetallic compounds in Al 6016/IF-steel friction stir spot welds. *Materials Science and Engineering A* **2010**, *527*, 4505–4509.

[22] Watanabe, T.; Takayama, H.; Yanagisawa, A. Growth manner of intermetallic compound layer produced at welding interface of friction stir spot welded aluminum/steel lap joint. *Materials Transactions* **2011**, *52*, 953–959.

[23] Shen, Z.; Chen, Y.; Haghshenas, M.; Gerlich, A.P. Role of welding parameters on interfacial bonding in dissimilar steel/aluminum friction stir welds. *Engineering Science and Technology, an International Journal* **2015**, *18*, 270–277.

[24] Pourali, M.; Abdollah-Zadeh, A.; Saeid, T.; Kargar, F. Influence of welding parameters on intermetallic compounds formation in dissimilar steel/aluminum friction stir welds. *Journal of Alloys and Compounds* **2017**, *715*, 1–8.

[25] Qiu, R.; Shi, H.; Zhang, K.; Tu, Y.; Iwamoto, C.; Satonaka, S. Interfacial characterization of joint between mild steel and aluminum alloy welded by resistance spot welding. *Materials Characterization* **2010**, *61*, 684–688.

[26] Yin, Y.H.; Sun, N.; North, T.H.; Hu, S.S. Hook formation and mechanical properties in AZ31 friction stir spot welds. *Journal of Materials Processing Technology* **2010**, *210*, 2062–2070.

[27] Zhang, D.; Shibayanagi, T. Material flow during friction stir spot welding of dissimilar Al2024/Al materials. *Materials Science and Technology* **2015**, *31*, 1077–1087.

[28] Li, Z.; Yue, Y.; Ji, S.; Chai, P.; Zhou, Z. Joint features and mechanical properties of friction stir lap welded alclad 2024 aluminum alloy assisted by external stationary shoulder. *Materials and Design* **2016**, *90*, 238–247.

[29] Chen, K.; Liu, X.; Ni, J. Keyhole refilled friction stir spot welding of aluminum alloy to advanced high strength steel. *Journal of Materials Processing Technology* **2017**, *249*, 452–462.

[30] Piccini, J.M.; Svoboda, H.G. Tool geometry optimization in friction stir spot welding of Al-steel joints. *Journal of Manufacturing Processes* **2017**, *26*, 142–154.

[31] Tasan, C.C.; Diehl, M.; Yan, D.; Bechtold, M.; Roters, F.; Schemmann, L.; Zheng, C.; Peranio, N.; Ponge, D.; Koyama, M.; et al. An overview of dual-phase steels: advances in microstructure-oriented processing and micromechanically guided design. *Annual Review of Materials Research* **2015**, *45*, 391–431.

[32] Radwanski, K.; Kuziak, R.; Rozmus, R. Structure and mechanical properties of dual-phase steel following heat treatment simulations reproducing a continuous annealing line. *Archives of Civil and Mechanical Engineering* **2019**, *19*, 453–468.

[33] Kalhor, A.; Soleimani, M.; Mirzadeh, H.; Uthaisangsuk, V. A review of recent progress in mechanical and corrosion properties of dual phase steels. *Archives of Civil and Mechanical Engineering* **2020**, *20*, 85.

[34] Feng, Z.; Santella, M.L.; David, S.A.; Steel, R.J.; Packer, S.M.; Pan, T.Y.; Kuo, M.; Bhatnagar, R.S. Friction stir spot welding of advanced high-strength steels - a feasibility study. *SAE Technical Paper* **2005**, 2005-01-1248.

[35] Hovanski, Y.; Santella, M.L.; Grant, G.J. Friction stir spot welding of hot-stamped boron steel. *Scripta Materialia* **2007**, *57*, 873–876.

[36] Das, H.; Mondal, M.; Hong, S.T.; Lim, Y.; Lee, K.J. Comparison of microstructural and mechanical properties of friction stir spot welded ultra-high strength dual phase and complex phase steels. *Materials Characterization* **2018**, *139*, 428–436.

[37] Rong, Z.; Li, L.; Chen, L.; Yuan, H.; Zhu, S.; Sun, Y.; Guan, S. Effect of Zn coating layer on the microstructure and mechanical properties of friction stir spot welded galvanized DP590 high-strength steel plates. *International Journal of Advanced Manufacturing Technology* **2021**, *113*, 1787–1798.

[38] Saeid, T.; Abdollah-Zadeh, A.; Shibayanagi, T.; Ikeuchi, K.; Assadi, H. On the formation of grain structure during friction stir welding of duplex stainless steel. *Materials Science and Engineering A* **2010**, *527*, 6484–6488.

[39] Emami, S.; Saeid, T.; Khosroshahi, R.A. Microstructural evolution of friction stir welded SAF 2205 duplex stainless steel. *Journal of Alloys and Compounds* **2018**, *739*, 678–689.

[40] Chen, W.; Wang, J.; Li, J.; Zheng, Y.; Li, H.; Liu, Y.; Han, P. Effect of the rotation speed during friction stir welding on the microstructure and corrosion resistance of SAF 2707 hyper duplex stainless steel. *Steel Research International* **2018**, *89*, 1700425.

[41] Wang, W.; Hu, Y.; Wu, T.; Zhao, D.; Zhao, H. Effect of rotation speed on microstructure and mechanical properties of friction-stir-welded 2205 duplex stainless steel. *Advances in Materials Science and Engineering* **2020**, *2020*, 5176536.

[42] Haghshenas, M.; Abdel-Gwad, A.; Omran, A.M.; Gökçe, B.; Sahraeinejad, S.; Gerlich, A.P. Friction stir weld assisted diffusion bonding of 5754 aluminum alloy to coated high strength steels. *Materials and Design* **2014**, *55*, 442–449.